November 13, 2018
Volume 51
Number 21

Macromolecules

pubs.acs.org/Macromolecules

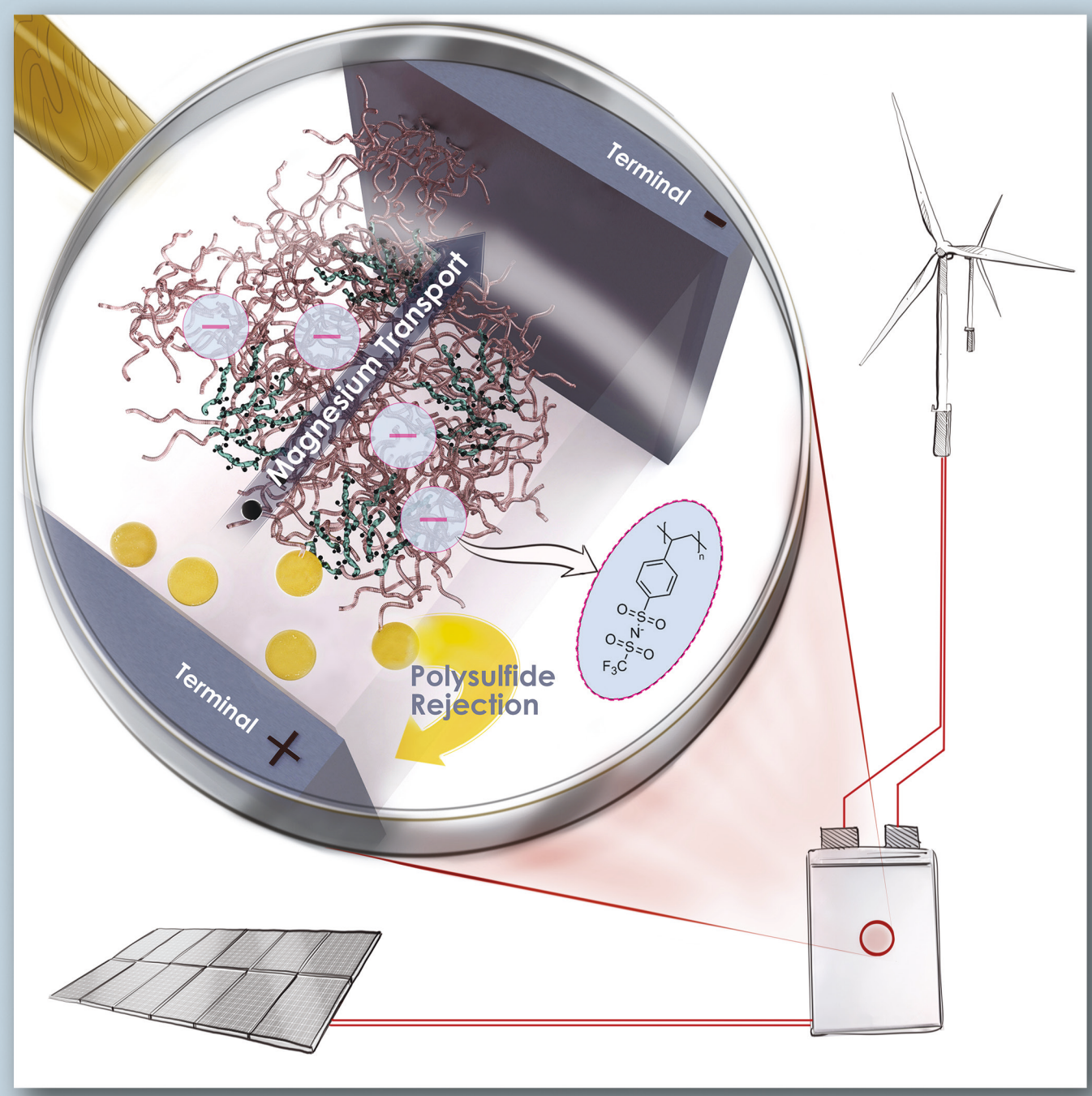

Macromolecules

Cite This: Macromolecules 2018, 51, 8629−8636

Article

pubs.acs.org/Macromolecules

Cross-Linked Ionomer Gel Separators for Polysulfide Shuttle Mitigation in Magnesium−Sulfur Batteries: Elucidation of Structure−Property Relationships

Hunter O. Ford, Laura C. Merrill, Peng He, Sunil P. Upadhyay, and Jennifer L. Schaefer*

Department of Chemical and Biomolecular Engineering, University of Notre Dame, Notre Dame, Indiana 46556, United States

Supporting Information

ABSTRACT: Cross-linked ionomer networks of varying poly(ethylene glycol) diacrylate cross-linker chain length, ionic comonomer chemistry, and comonomer ratio have been studied for their use as polysulfide shuttle inhibiting separators in magnesium−sulfur (Mg−S) batteries. Through the use of X-ray scattering, polysulfide diffusion experiments, conductivity measurements, and Mg−S cell cycling, it was determined that inclusion of tethered anions in polymer networks mitigates the polysulfide shuttle effect. Polysulfide crossover through networks into a bulk electrolyte can be reduced by absorption into the polymer gel, steric rejection, and electrostatic rejection, with the predominance of these mechanisms dictated by polymer composition and structure. The best network composition allowed an initial Mg−S cell discharge capacity of 522 mAh/g compared to a discharge capacity of 365 mAh/g using a literature standard glass fiber separator. The ionomer cell saw 67% capacity retention after three cycles, whereas the glass fiber separator could not complete the first charging cycle due to the polysulfide shuttle.

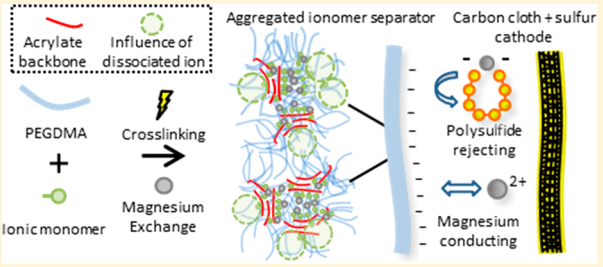

INTRODUCTION

To meet the energy storage needs of the future, the development of a wide array of rechargeable battery chemistries is of paramount importance. Of specific interest are systems capable of delivering high energy density safely and at practical cost, thereby enabling the electrification of transportation. Fully electric transportation, coupled with a rise in sustainable energy generation, will help to mitigate the effects of climate change via a reduction in fossil fuel usage. One such high energy density system is the magnesium sulfur (Mg−S) battery, offering a high theoretical volumetric energy capacity of 3200 Wh/L. In addition, magnesium and sulfur are both abundant and low-cost materials, making them an ideal choice for a sustainable battery technology.

Like all metal−sulfur batteries, the Mg−S system suffers from a phenomenon known as the polysulfide shuttle effect. During the operation of the Mg−S system, intermediate species, magnesium polysulfides (MgPS), are generated and consumed in the sulfur cathode. MgPS can diffuse away from the cathode and during the charging process become reduced at the magnesium metal anode, either irreversibly adhering to the surface or returning to the cathode to repeat the redox shuttle. This process leads to the formation of a passivating layer on the anode, loss of active material, and poor cycle efficiency.[1] The polysulfide shuttle effect results in dramatic capacity fading and short lifetimes of the Mg−S cell, precluding the practical use of this battery system.

Since the demonstration of the first Mg−S cell, much attention has been focused on mitigating the polysulfide shuttle effect to prolong cell capacity. Sulfur has been incorporated into high surface area graphene,[2] mesoporous carbon structures,[3] carbon nanofiber (CNF) interlayer cathodes,[4] and graphidiyne cages.[5] In addition, it has been shown that the polysulfide shuttle effect can be lessened by reducing the solubility of polysulfides and sulfur in the electrolyte by increasing the electrolyte salt concentration.[6] While these approaches have been successful, it is desirable to explore additional means of further mitigating the polysulfide shuttle effect to allow practical use of Mg−S cells.

In the Li−S literature, reported attempts to mitigate the polysulfide shuttle effect are numerous, with many studies employing materials that alter polysulfide transport via chemical interactions or selective polysulfide rejection.[7−11] Strategies specifically involving polymers include encapsulation of sulfur particles with conductive polymers, the use of specialty cathode binders, and application of ionomers with electrostatic polysulfide rejection mechanisms.[12−18] The use of polymeric coatings on sulfur cathodes and separators has dramatically improved performance in Li−S cells, yet none have eliminated the presence of polysulfides in the electrolyte. Notably, there has been limited study of correlations between the structure of sulfur cathode polymeric functional layers and polysulfide transport.

Herein we report on a class of polymers capable of impacting and mitigating the polysulfide shuttle effect in Mg−S cells. The polymers are cross-linked ionomeric networks

Received: August 8, 2018
Revised: October 5, 2018
Published: October 22, 2018

DOI: 10.1021/acs.macromol.8b01717
Macromolecules 2018, 51, 8629−8636

that effectively repel polysulfides via physical and electrostatic mechanisms. Poly(ethylene glycol) diacrylate or dimethacrylate (PEGDA/PEGDMA) is copolymerized with an ionic monomer, resulting in a cross-linked network of tethered anionic groups bridged by PEG linkers. When swelled in an electrolyte, some degree of the ionic groups undergo dissociation. The resultant network consisting of tethered negative charges is hypothesized to facilitate cationic conduction while also minimizing the polysulfide shuttle effect due to electrostatic exclusion of the negatively charged polysulfide anions.

An effort to understand the fundamentals governing ion transport in these systems has been made, in the hopes that such an understanding will lead to the engineering of better materials for Mg−S and other metal−sulfur systems. The effects of PEG linker length, tethered anion chemistry, and charge:ether oxygen ratio (Ch:EO) on ion transport and material structure are investigated. Conductivity measurements, small-angle X-ray scattering (SAXS) analyses, polysulfide diffusion experiments, and cell cycling tests have been employed to provide a comprehensive picture of structure−composition−property relationships. It is found that with an increase in bound charge content (Ch:EO) the electrolyte swelled networks become less conductive to cationic species but also more greatly restrict polysulfide transport. The rejection of polysulfide species is shown to be a result of two distinct mechanisms—electrostatic repulsion and physical restriction—with the best performing films taking advantage of both mechanisms while balancing cationic conductivity. A series of Mg−S cells with ionomer separators exhibit a variety of discharge capacities and capacity retention as a function of film composition.

EXPERIMENTAL SECTION

Preparation of Self-Supporting Films. Poly(ethylene glycol) diacrylate (PEGDA) (M_n = 700 g/mol) (Sigma-Aldrich) is washed first with *n*-hexanes (Sigma-Aldrich) and then pentane (Sigma-Aldrich) to remove stabilizers. Poly(ethylene glycol) dimethacrylate (PEGDMA) (M_n = 1000 g/mol) (Polysciences, Inc.) is used as received. The ionic monomer sodium 4-vinylbenzenesulfonate (NaSS) (>90% technical, Sigma-Aldrich) is used as received, and the ionic monomer potassium 4-styrenesulfonyl(trifluoromethanesulfonyl)imide (KSTFSI) is synthesized according to Armand et al.[19] Magnesium metal is purchased from Gallium Source. Structures for PEGDA, PEGDMA, NaSS, and KSTFSI are presented in Figure 1a−d.

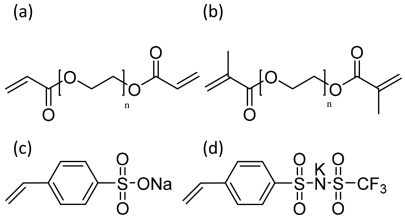

Figure 1. Monomers used in ionomer fabrication (a) PEGDA, (b) PEGDMA, (c) NaSS, and (d) KSTFSI.

In ambient conditions, the PEGDA/PEGDMA monomer of a given chain length and a given ionic monomer are dissolved in dimethyl sulfoxide (DMSO) (Sigma-Aldrich). The photoinitiator 2-hydroxy-4′-(2-hydroxyethoxy)-2-methyl propiophenone (Sigma-Aldrich) is added to the solution, which is then stirred. The solution of monomers, photoinitiator, and DMSO is then sandwiched between two 1/4 in. thick borosilicate glass plates (McMaster Carr) separated by 200 μm thick glass microscope slides (VWR), which are placed in a UVC-515 ultraviolet multilinker 254 nm UV oven. The films are photo-cross-linked for a total of 45 min. The resultant polymers are washed with 18 MΩ deionized water to remove unreacted material. The films are then placed in a stirred aqueous ion exchange solution of 0.5 M magnesium chloride to achieve magnesiated forms of the polymer. The ion exchange solution is replaced every 12 h for 48 h, after which free salt is washed from the films by repeating the same process but with pure deionized water. The films are air-dried, brought into an argon-filled glovebox, and vacuum-dried for 24 h at 80 °C to remove residual moisture. Ion exchange is confirmed via inductively coupled plasma-optical emission spectroscopy (ICP-OES).

Samples are referenced by the PEGDA/PEGDMA monomer with the number of repeat units, followed by the ionic monomer denotation and then the Ch:EO ratio. For example, a film produced with PEGDA of M_n = 700 g/mol and STFSI at the ratio of Ch:EO = 0.007 would be referenced as $PEG_{13}DA\_x\_STFSIMg\_7$.

Conductivity Measurements. Conductivity is measured on samples of swelled polymer films sandwiched between brass electrodes with a Novocontrol broadband dielectric spectrometer equipped with a cryostat and Quatro temperature control system. Samples are swelled to equilibrium and then secured into the sample cell while in the glovebox.

Ultradry Solvent Preparation. All solvents used in electrochemical tests, H-cell experiments, and UV/vis experiments are dried to less than 10 ppm moisture as confirmed by Karl Fischer titration. For tetrahydrofuran (THF, anhydrous, Sigma-Aldrich), this is achieved by storing over 3 Å molecular sieves. For 1,2-dimethoxyethane (DME, 99.5% anhydrous, Sigma-Aldrich), this is achieved by distillation over calcium hydride then storage on molecular sieves.

H-Type Diffusion Experiments. A section of polymer film to be tested is allowed to swell in anhydrous THF. The swelled film is then placed between the two halves of the H-cell. To one side of the H-cell, 3 mL of a magnesium polysulfide solution is added, while simultaneously 3 mL of neat electrolyte is added to the opposite side. The cell is left for 24 h, after which the solution on the side into which MgPS diffuse is collected and analyzed via UV/vis spectroscopy. The H-cell electrolyte is prepared according to the literature.[20] A solution of the molar ratio 1:4 magnesium bis(hexamethyl disilazide) ($Mg(HMDS)_2$) (>97%, Sigma-Aldrich) to magnesium chloride ($MgCl_2$) (>99.9%, anhydrous, Aldrich), 0.5 M with respect to total magnesium content, is created by dissolving $Mg(HMDS)_2$ in anhydrous THF and then adding $MgCl_2$ and allowing to equilibrate. Magnesium polysulfide solutions are prepared by adding 0.0144 g of elemental sulfur (Aldrich) to 3 mL of the aforementioned $Mg(HMDS)_2$−$MgCl_2$ electrolyte solution and stirring. The solution color quickly changes from pale yellow, to light blue, to a deep yellow after 2 h of equilibration. It is then used in the H-cell. Eventually, continued reaction yielded a white precipitate; however, the MgPS solutions are stable long enough to be used in the 24 h H-cell experiment, with precipitate only being formed after a few days of solution equilibration.

Small/Wide-Angle X-ray Scattering (SAXS/WAXS). Polymer samples are loaded into capillary tubes in an argon-filled glovebox and then swelled with solvent. The tubes are sealed within the glovebox to prevent solvent evaporation and incorporation of moisture into the polymer sample. SAXS/WAXS measurements are obtained using the Argonne APS synchrotron beamline 12-ID-B, operated by the Chemical and Materials Science group at Argonne National Laboratory, with an X-ray beam wavelength of 0.9322 Å (energy of 13.3 keV).

Ultraviolet/Visible (UV/Vis) Spectroscopy. Samples are prepared in 10 × 1 mm quartz microcuvettes (Type 46 Firefly Sciences) in an argon-filled glovebox. The cuvette is sealed and then measured using a Jasco V-670 UV−vis−near-IR spectrometer, from 212 nm (cutoff wavelength for THF) to 650 nm.

Cathode Preparation and Cell Cycling. A 0.35 M (with respect to Mg) THF-based electrolyte containing 1:2 $Mg(HMDS)_2$:$AlCl_3$ is

DOI: 10.1021/acs.macromol.8b01717
Macromolecules 2018, 51, 8629−8636

prepared according to the literature.[21] Likewise, a 0.25 M (with respect to $Mg(TFSI)_2$) DME-based electrolyte containing 1:2 $Mg(TFSI)_2$:$MgCl_2$ is prepared according to literature and used unconditioned.[6] Sulfur is incorporated into high surface area activated carbon cloth (ACC) (Ceramaterials FM10) discs, 0.5 mm thick and 1 cm in diameter, by two different methods depending on the electrolyte to be used. For the DME-based electrolyte, within the glovebox a solution of sulfur dissolved in THF is added to the ACC such that when the THF was evaporated, the sulfur loading is 1 mg/cm^2. For the THF-based electrolyte, inside the glovebox 4 mg of sulfur is spread onto a ACC disc, which is then loaded in a Teflon vessel which is sealed inside a stainless steel reactor. The reactor is then held at 155 °C for 12 h. The additional sulfur is required for the THF-based electrolytes to prevent complete sulfur dissolution into the large amount of electrolyte needed to fully wet the cathode and separator. Structures for $Mg(HMDS)_2$ and $Mg(TFSI)_2$ are presented in Figure 2a,b.

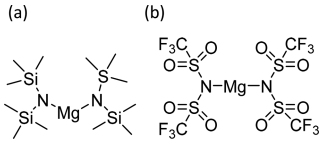

Figure 2. Magnesium electrolyte salts (a) $Mg(HMDS)_2$ and (b) $Mg(TFSI)_2$.

The cathodes are assembled in coin-type cells with the cathode supported in a Teflon donut (to prevent cathode dewetting when the cell was crimped), glass fiber (Whatman) or ionomer film as a separator, Mg metal anode with freshly removed oxide layer, 160 μL of electrolyte, and stainless steel spacers and wave spring. Mg foil is cleaned via mechanical scraping immediately prior to use. Cells are rested 2 h before initial discharge and are tested at a rate of 0.005 C with respect to sulfur on a Neware Battery Tester Systems battery tester.

RESULTS AND DISCUSSION

Structural Determination via Small-Angle X-ray Scattering (SAXS). To elucidate the structure−property relationships of this class of ionomer networks, morphology is probed with the use of SAXS. Scattering spectra for THF swelled $PEG_{20}DMA$ and $PEG_{13}DA$ ionomers with varying Ch:EO and anion chemistry are presented in Figures 3a and 3b, respectively. For a given scattering spectra, a local maximum in scattering intensity, q_x, can be used to determine the average distance between the structures responsible for the scattering, d_x, by means of the Bragg condition, where $q_x = 2\pi/d_x$.[22] A sharper local maximum indicates a more monodisperse set of length scales that give rise to the observed average length scale.

In the case of the pure PEGDA/PEGDMA films, the acrylate backbones segregate, producing acrylate-rich and acrylate-poor regions.[23−25] Peaks q_a and q_c are assigned to the correlation length between acrylate-rich clusters. Secondary peaks q_b and q_d are indicative of moderate range order between scattering structures—a phenomenon that is observed in many types of multidomain soft matter and is a result of imperfect ordering over large unit cells.[26] Note the characteristic distance between acrylate backbones is shorter in the $PEG_{13}DA$ case due to the shorter cross-linker length. By steric necessity, the portion of the PEG chains that are attached to the acrylate backbones is more extended and densely packed compared to the acrylate-poor regions where there is substantial chain looping. A schematic of this proposed structure is presented in Figure 4a. Considering the spacing between chains as the pore

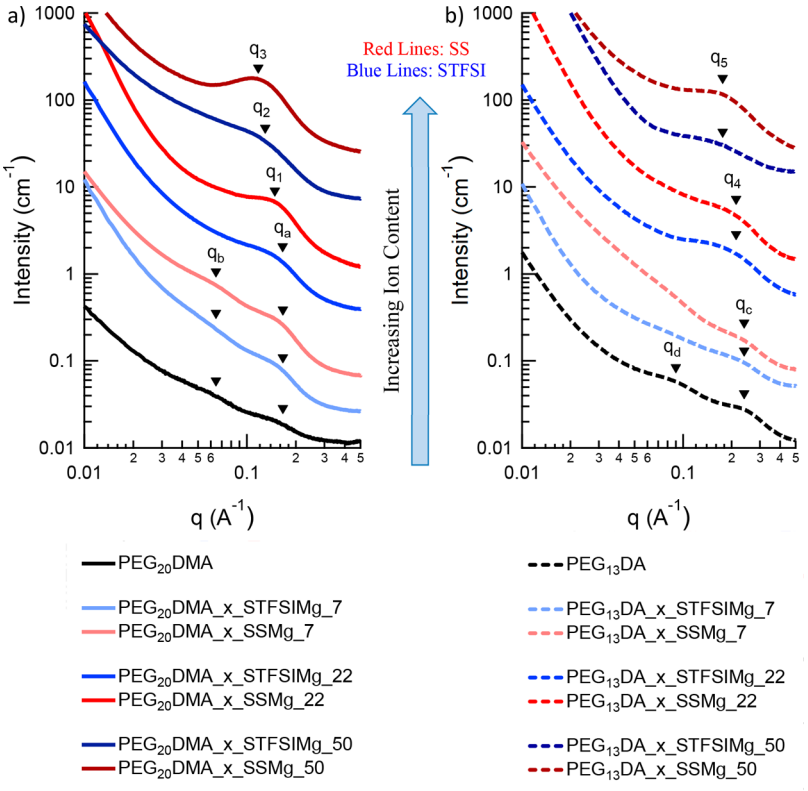

Figure 3. SAXS spectra for $PEG_{20}DMA$ (a) and $PEG_{13}DA$ (b) ionomers of varying anion chemistry and Ch:EO. Samples are swelled in THF and analyzed at room temperature (23 °C). Spectra are shifted vertically for clarity.

DOI: 10.1021/acs.macromol.8b01717
Macromolecules 2018, 51, 8629−8636

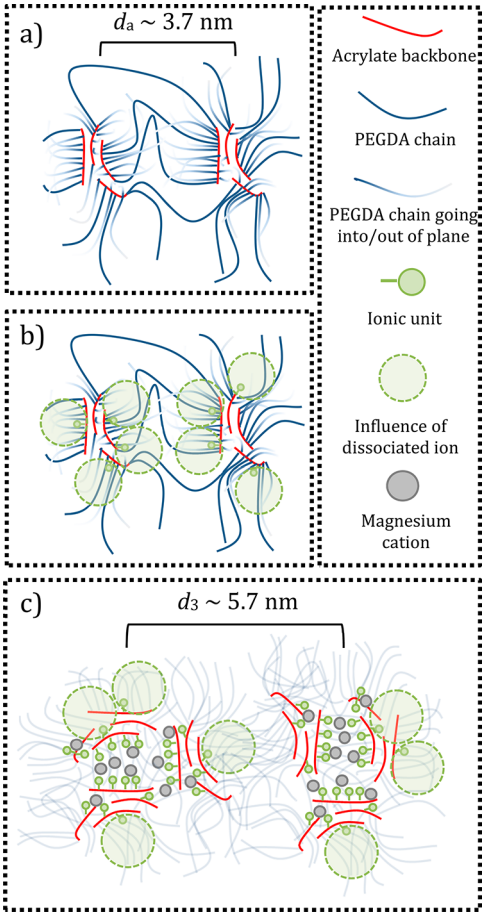

Figure 4. Schematic detailing proposed morphology of (a) pure PEGDA/PEGDMA films, (b) unaggregated films containing ionic units, and (c) aggregated ionomer films. Pictured as a two-dimensional representation, chains with a color gradient are going into and out of the plane. For clarity, PEG chains are lightened in box c.

size, a proportional averaging of the acrylate-rich and acrylate-poor regions constitutes an effective pore size. With comparable acrylate domain sizing, the $PEG_{20}DMA$ films have a larger portion of the acrylate-poor region, yielding a larger effective pore size relative to $PEG_{13}DA$ films.

In the case of the lowest charge content, Ch:EO = 0.007, ionic units have been incorporated without a measurable change in the material structure as depicted in Figure 4b, indicating a high degree of dissociation of the ionic units. The tethered dissociated anions create regions influenced by negative charge, the range of which is determined by the Debye length of the swelling solvent and/or electrolyte.

Moderate to high Ch:EO ratios result in ionic aggregation as depicted in Figure 4c, indicated by the evolution of the characteristic ionomer peak with increasing Ch:EO (peaks q_1–q_5) and an increase in distance between scattering structures.[27] It appears that for ionic aggregation to occur, some critical number of associated ionic groups must be present in the material, a number that also seems to be a function of PEG cross-linker length. In regards to Ch:EO = 0.022, the threshold has been crossed for $PEG_{13}DA$ samples of both anion types, evidenced by the shift of q_4 relative to q_c. At this same Ch:EO the $PEG_{20}DMA$ samples are just on the cusp of aggregation. The more associated SS sample shows a slight length scale shift; the more dissociated STFSI sample has not shifted in length scale relative to q_a. The differences in morphology are most pronounced at Ch:EO = 0.050, where the difference in anion dissociability significantly impacts the total number of associated ionic groups and therefore degree of aggregation.

In general, samples with the STFSI anion experience a lower degree of length scale shift and have broader correlation peaks, indicating a lesser degree of aggregation. Because of its electron delocalizing nature, the STFSI anion has been shown to have a lower ion pair binding energy relative to the SS anion,[28] which promotes ion pair dissociation and leads to differences in aggregation degree and transport properties. Further discussion concerning the relationship of ion dissociation and degree of aggregation is found in the Supporting Information.

It is likely that the ionic aggregates are surrounded by densely packed PEG sheaths, with the interaggregate distance determined by the size of the aggregate and corresponding polymer shell.[29,30] The dense packing of PEG chains around the aggregates and the greater extension of any chains bridging between aggregates (due to the larger distance between scattering structures relative to pure the PEGDA/PEGDMA case) leads to a decrease in free volume and therefore effective pore size. Unfortunately, the X-ray scattering length density contrast between PEG chains and THF is not high enough to directly observe pore size. However, the results from the conductivity and MgPS diffusion experiments support the claim that effective pore size decreases with greater aggregation and shorter cross-linker length.

DC Conductivity. The conductivity of the ionomers is studied in an effort to understand the compositional impact on cation transport. The dc conductivity values for pure THF swelled $PEG_{20}DMA$ and $PEG_{13}DA$ ionomers with varying Ch:EO and anion chemistry are presented in Figure 5.

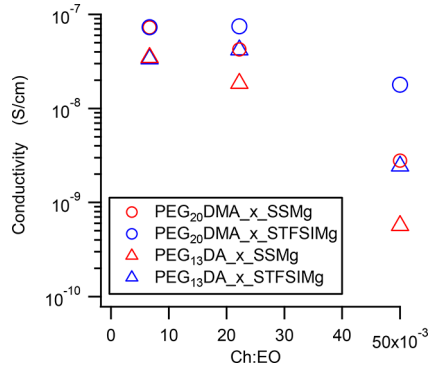

Figure 5. DC conductivity of THF swelled ionomers of varying cross-linker length, anion chemistry, and Ch:EO.

Conductivity decreases as the effective pore size decreases. As either a result of cross-linker length or aggregation, the increased steric hindrance inhibits transport of solvated cation complexes. As the Ch:EO increases, differences in conductivity due to varying anion dissociability become noticeable, especially in the highest Ch:EO compositions where the SS samples are highly aggregated and the STFSI films less so.

To verify suitable conductivity for full cell operation, a select set of films are swelled in two different Mg–S compatible electrolyte systems, with the results presented in Figure 6.

In the ionomer films, the bulkier HMDS-containing complexes make the THF-based electrolyte more than an order of magnitude less conductive than the DME electrolyte,

DOI: 10.1021/acs.macromol.8b01717
Macromolecules 2018, 51, 8629–8636

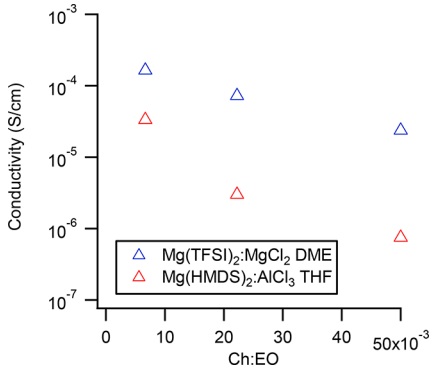

Figure 6. Conductivity of $PEG_{13}DA\_x\_STFSIMg$ films swelled with two electrolytes relevant for Mg−S batteries.

even though the liquid electrolytes themselves are of comparable conductivity (15 and 4.3 mS/cm for the DME- and THF-based electrolytes, respectively). The conductivity of the DME electrolyte swelled samples, except for the highest Ch:EO, meet the accepted bare minimum of conductivity for practical use, 1×10^{-4} S/cm. Although both electrolytes are eventually used in full Mg−S cells, cells with the THF-based electrolyte are not fully functioning due to the inherent low conductivity.

Magnesium Polysulfide Exclusion. The effect of cross-linker length, anion chemistry, and Ch:EO ratio on the ability of a given film to exclude MgPS is examined with the use of an H-style diffusion cell, as shown in Figure 7. Figure 8 displays

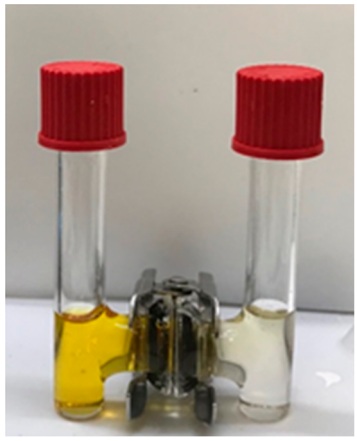

Figure 7. H-style diffusion cell containing MgPS in a THF-based electrolyte on the left-hand side, the same electrolyte without added sulfur on the right-hand side, and the film to be tested in between. Pictured is the H-cell containing a $PEG_{20}DMA$ film 2 h after assembly.

the UV/vis background-subtracted absorption spectra for solutions collected from H-cells run with various ionomer films, where here the background is taken to be the pristine electrolyte solution. The observed negative absorbance is elaborated upon in the Supporting Information but briefly is a result of depletion of (absorbing) salts relative to the reference cuvette solution combined with low MgPS crossover.

Total polysulfide crossover clearly decreases with shorter cross-linker lengths and ionomer aggregation. Although the exact speciation of the polysulfides in solution is not known, a decrease in the wavelength of maximum absorbance corresponds to a lower average chain length polysulfide population (further discussion on this point in the Supporting Information, Figure S5). Observation of the predominant crossover of shorter chain polysulfides in the case of aggregated and/or short cross-linker films is direct evidence that such films have smaller effective pore sizes. Comparing the $PEG_{20}DMA\_x\_SSMg\_22$ to $PEG_{20}DMA\_x\_STFSIMg\_22$, the former excludes MgPS to a greater degree due to the onset of ionic aggregation in the film as seen in the SAXS. Comparing $PEG_{20}DMA\_x\_SSMg\_50$ and $PEG_{20}DMA\_x\_STFSIMg\_50$, the striking difference in absorbance is due to ion pair dissociation. Both samples are aggregated leading to physical restriction of MgPS; however, $PEG_{20}DMA\_x\_STFSIMg\_50$ has a greater degree of ion pair dissociation, which offers additional MgPS restriction via electrostatic rejection.

Concerning the electrostatic rejection of polysulfides, the effective pore size of the material must be reasonably comparable (certainly within an order of magnitude) to the Debye screening length to have an appreciable effect. This explains the apparent contradictory effect of ionic units on the restriction capability of nonaggregated $PEG_{13}DA$ and $PEG_{20}DMA$ films. In the case of the low Ch:EO $PEG_{20}DMA$ films, the effective pore size must be large enough that the charge on a tethered anion can be screened with ample space left in the pore for a polysulfide anion to diffuse unhindered. Hence, substituting ineffective ionic units for PEG chains results in the observed greater polysulfide crossover (i.e., $PEG_{20}DMA\_x\_STFSIMg\_7$ vs. $PEG_{20}DMA$). In contrast, when the pore size is small enough (all $PEG_{13}DA$ and $PEG_{20}DMA\_x\_STFSIMg\_50$ films) electrostatic repulsion of polysulfide anions may be observed.

The $PEG_{13}DA\_x\_STFSIMg$ compositions display a highly varied response to the MgPS solution, as can be seen by the films exposed to the H-cell solution pictured in Figure 9. As the Ch:EO increases, the mechanism of polysulfide crossover mitigation changes, from that of absorptive trapping (pure $PEG_{13}DA$), to a degree of electrostatic rejection ($PEG_{13}DA\_x\_STFSIMg\_7/22$), to a combination of electrostatic and small pore size rejection ($PEG_{13}DA\_x\_STFSIMg\_50$).

Mg−S Cell Cycling. A series of Mg−S cells using the $PEG_{13}DA\_x\_STFSIMg$ films of varying Ch:EO as separators are assembled and cycled to study the impact on cell performance. Two electrolytes are studied: $Mg(HMDS)_2$:$AlCl_3$ in THF and $Mg(TFSI)_2$:$MgCl_2$ in DME. The potential curves as a function of capacity are presented in Figure 10 for Mg−S cells employing the DME-based electrolyte. Cells with the THF-based electrolyte had poor initial discharge capacity and essentially nonexistent charging capacity, with data shown in Figures S5 and S6.

The initial discharge capacity appears highly correlated to the polysulfide rejecting capability of the separator used. When polysulfides are unable to diffuse away from reduction sites on the cathode, the active material utilization and hence discharge capacity are enhanced. The charging capacity also follows the same trend, with the exception of the glass fiber separator and the highest Ch:EO ionomer.

Cells with glass fiber separators are not able to charge to a preset cutoff potential, instead suffering continual "charging" at a given potential ~2 V followed by eventual fluctuations in potential. The continual charging indicates such cells suffer from a serious polysulfide shuttle effect in which the reduction

DOI: 10.1021/acs.macromol.8b01717
Macromolecules 2018, 51, 8629−8636

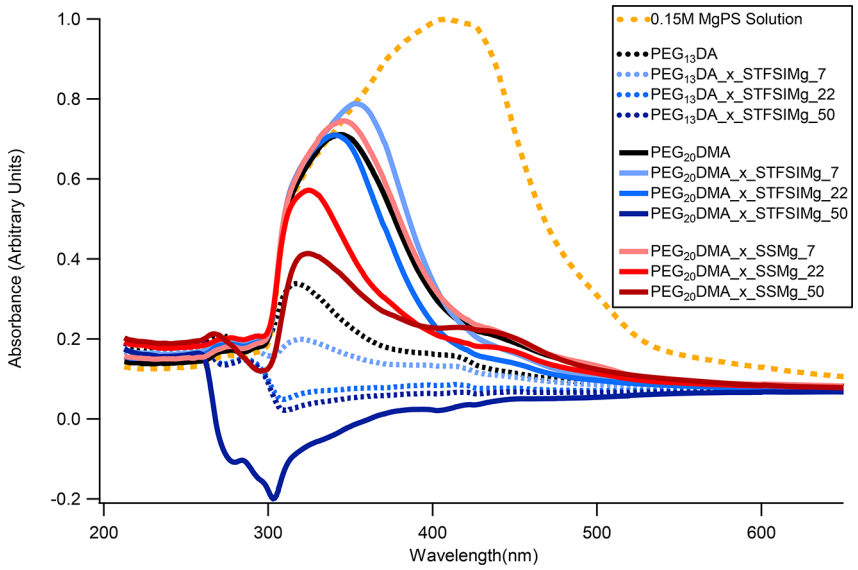

Figure 8. UV/vis absorption spectra of polysulfide crossover solutions for $PEG_{20}DMA$ and $PEG_{13}DA$ films of varying Ch:EO and anion chemistry.

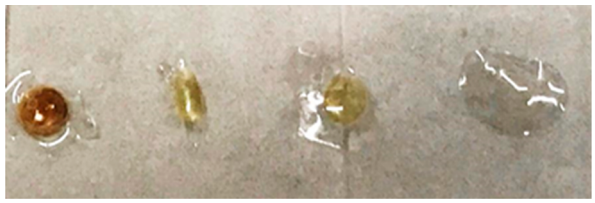

Figure 9. $PEG_{13}DA$ films recovered from diffusion cell experiments. From left to right Ch:EO is 0, 7, 22, and 50.

and oxidation of polysulfides are balanced at each electrode, thereby maintaining a constant potential. The simple fact that all of the cells with polymer separators can reach a designated cutoff potential indicates that they are capable of mitigating the shuttle effect to some extent.

With regard to the $PEG_{13}DA\_x\_STFSIMg\_50$ cell, the charging capacity is markedly lower than the other $PEG_{13}DA$ cells. This is hypothesized to be due to the low ionic conductivity of this film, which results in premature termination of charging. This demonstrates that for practical application the best performing ionomer balances the ability to restrict MgPS but also conduct the active cation species.

The discharge curve of each cell contains two distinct plateaus, ~1.4 and 0.8 V, with some cells exhibiting a third plateau near the discharge cutoff potential. The composition of the separator appears to impact not only the total discharge capacity but also the capacity of each plateau. The first plateau is assigned to the reduction of sulfur into soluble higher order polysulfides. The lower Ch:EO ionomers, having larger pore sizes relative to the highest Ch:EO ionomer, absorb some of the higher order polysulfides. The glass fiber separator (being macroporous) and the $PEG_{13}DA\_x\_STFSIMg\_50$ separator, having the smallest effective pore size of all the ionomers, do not strongly absorb the larger higher order polysulfides.

The accessibility of the higher order polysulfides during the second reduction step determines the capacity of the second plateau. In the case of the glass fiber separator, the higher order species can diffuse back to the cathode to become reduced. In the case of the $PEG_{13}DA\_x\_STFSIMg\_50$ separator the higher order polysulfides always remain close to the cathode reaction site, thus allowing for a greater utilization of the active

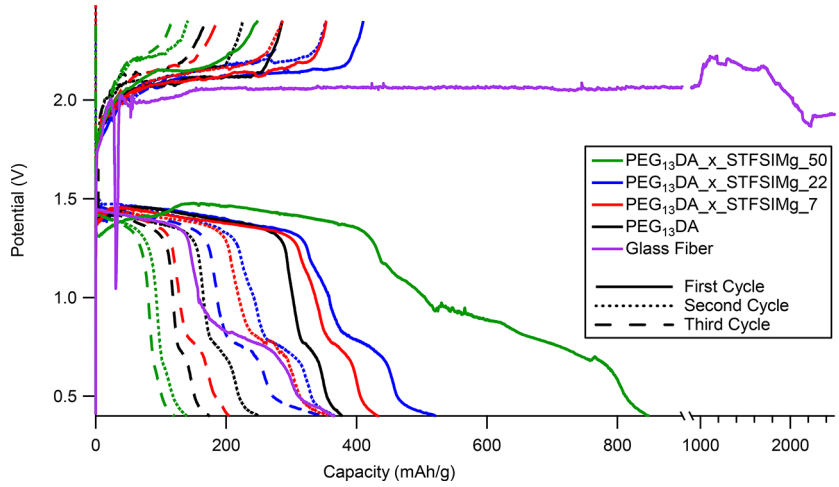

Figure 10. Discharge/charge potential curves for Mg−S cells with varying separator material.

DOI: 10.1021/acs.macromol.8b01717
Macromolecules 2018, 51, 8629−8636

material and subsequent capacity increase on the first discharge cycle relative to the other ionomers.

It is possible that the third plateau is the result of polysulfides that had been absorbed in the separator migrating to the cathode to become reduced. This is most likely to occur at the end of the discharge cycle due to the establishment of a concentration gradient after polysulfides in the cathode have been consumed while polysulfides in the separator have not.

Although the issue of capacity fading upon cycling is not completely mitigated, films that balance MgPS restriction and cationic conductivity see improved capacity retention. After three cycles, the capacity retention of the $PEG_{13}DA\_x\_STFSIMg\_22$, $PEG_{13}DA\_x\_STFSIMg\_7$, and pure $PEG_{13}DA$ cells are 66.9%, 47.2%, and 46.1% of initial, respectively. Mechanisms of capacity fade include loss of active material due to absorption of sulfur species into the separator and, likely, the poor kinetics associated with upgrading lower order polysulfides and MgS during the charge cycle.[31,32]

As shown previously in Figure 9, polysulfide crossover in the diffusion H-cells is partially mitigated by absorption into the films—a phenomenon that prevents the shuttle effect in full cells but also contributes to capacity fade. Post-mortem analysis of a full cell (Figure S8) confirms that polysulfide absorption does occur during cycling. Future studies should focus on the usage of materials as thin layered cathode coatings as opposed to bulk scale separators. Thin layer coatings will not absorb as much active material leading to better life cycle and will widen the range of applicable materials by loosening the conductivity requirements. Finally, we cannot rule out the incomplete oxidation of MgS during charging as a contributing factor to the capacity fade; this effect is known to be more severe for MgS than for Li_2S but is beyond the scope of this study.

CONCLUSIONS

A series of cross-linked ionomer films consisting of varying chain lengths, anion chemistry, and Ch:EO were synthesized. These materials were further characterized in terms of structure, conductivity, ability to repel MgPS, and performance enhancement of full Mg−S cells employing the ionomers as separators. It was confirmed that tethered anions could electrostatically repel negatively charged polysulfide anions in certain circumstances. Furthermore, it was determined that anion chemistry, in particular anion dissociability, plays a large part in controlling the ionomer structure and transport properties by modulating ionic aggregation within the film. In some cases, increase in tethered anion content results in significant ionic aggregation within the ionomer, which results in polysulfide crossover mitigation due to steric, rather than electrostatic, restriction. Relative to standard commercial glass fiber separators, the ionomer separators enhanced the performance of Mg−S cells in terms of discharge capacity and effectively suppressed the polysulfide shuttle effect. Although further work is required to improve cation transport and capacity retention, the elucidation of structure−composition−property relationships can hopefully guide the engineering of better materials for Mg−S and other metal−sulfur batteries.

ASSOCIATED CONTENT

Supporting Information

The Supporting Information is available free of charge on the ACS Publications website at DOI: 10.1021/acs.macromol.8b01717.

Supplementary SAXS spectra, conductivity measurements, UV/vis experiments, Mg−S cell cycling (PDF)

AUTHOR INFORMATION

Corresponding Author

*E-mail Jennifer.L.Schaefer.43@nd.edu; phone (574)-631-5114 (J.L.S.).

ORCID

Jennifer L. Schaefer: 0000-0003-4293-6328

Notes

The authors declare no competing financial interest.

ACKNOWLEDGMENTS

We thank Dr. Xiaobing Zuo from Argonne National Lab for assistance in collecting SAXS spectra, Dr. Ian Lightcap and the Notre Dame Materials Characterization Facility for UV/vis instrumentation, and Jon Loftus and the Notre Dame Center for Environmental Science and Technology for ICP-OES and ion chromatography instrumentation. This research used resources of the Advanced Photon Source, a U.S. Department of Energy (DOE) Office of Science User Facility operated for the DOE Office of Science by Argonne National Laboratory under Contract DE-AC02-06CH11357. Hunter O. Ford acknowledges financial support from The Society of Arthur J. Schmitt Fellows. The authors gratefully acknowledge funding from the National Science Foundation via Award CBET-1706370.

REFERENCES

(1) Kim, H. S.; Arthur, T. S.; Allred, G. D.; Zajicek, J.; Newman, J. G.; Rodnyansky, A. E.; Oliver, A. G.; Boggess, W. C.; Muldoon, J. Structure and Compatibility of a Magnesium Electrolyte with a Sulphur Cathode. *Nat. Commun.* **2011**, *2* (1), 427.

(2) Vinayan, B. P.; Zhao-Karger, Z.; Diemant, T.; Chakravadhanula, V. S. K.; Schwarzburger, N. I.; Cambaz, M. A.; Behm, R. J.; Kübel, C.; Fichtner, M. Performance Study of Magnesium-Sulfur Battery Using a Graphene Based Sulfur Composite Cathode Electrode and a Non-Nucleophilic Mg Electrolyte. *Nanoscale* **2016**, *8* (6), 3296−3306.

(3) Zhao-Karger, Z.; Zhao, X.; Wang, D.; Diemant, T.; Behm, R. J.; Fichtner, M. Performance Improvement of Magnesium Sulfur Batteries with Modified Non-Nucleophilic Electrolytes. *Adv. Energy Mater.* **2015**, *5* (3), 1401155.

(4) Yu, X.; Manthiram, A. Performance Enhancement and Mechanistic Studies of Magnesium-Sulfur Cells with an Advanced Cathode Structure. *ACS Energy Lett.* **2016**, *1* (2), 431−437.

(5) Du, H.; Zhang, Z.; He, J.; Cui, Z.; Chai, J.; Ma, J.; Yang, Z.; Huang, C.; Cui, G. A Delicately Designed Sulfide Graphdiyne Compatible Cathode for High-Performance Lithium/Magnesium−Sulfur Batteries. *Small* **2017**, *13* (44), 1702277.

(6) Gao, T.; Hou, S.; Wang, F.; Ma, Z.; Li, X.; Xu, K.; Wang, C. Reversible S0/MgSxRedox Chemistry in a MgTFSI2/MgCl2/DME Electrolyte for Rechargeable Mg/S Batteries. *Angew. Chem., Int. Ed.* **2017**, *56* (43), 13526−13530.

(7) Manthiram, A.; Fu, Y.; Chung, S. H.; Zu, C.; Su, Y. S. Rechargeable Lithium-Sulfur Batteries. *Chem. Rev.* **2014**, *114* (23), 11751−11787.

(8) Fan, X.; Sun, W.; Meng, F.; Xing, A.; Liu, J. Advanced Chemical Strategies for Lithium-Sulfur Batteries: A Review. *Green Energy Environ.* **2018**, *3* (1), 2−19.

DOI: 10.1021/acs.macromol.8b01717
Macromolecules 2018, 51, 8629−8636

(9) Huang, J. Q.; Zhuang, T. Z.; Zhang, Q.; Peng, H. J.; Chen, C. M.; Wei, F. Permselective Graphene Oxide Membrane for Highly Stable and Anti-Self-Discharge Lithium-Sulfur Batteries. *ACS Nano* **2015**, *9* (3), 3002−3011.
(10) Park, J.; Yu, B. C.; Park, J. S.; Choi, J. W.; Kim, C.; Sung, Y. E.; Goodenough, J. B. Tungsten Disulfide Catalysts Supported on a Carbon Cloth Interlayer for High Performance Li−S Battery. *Adv. Energy Mater.* **2017**, *7* (11), 1602567.
(11) Tao, X.; Wang, J.; Ying, Z.; Cai, Q.; Zheng, G.; Gan, Y.; Huang, H.; Xia, Y.; Liang, C.; Zhang, W.; et al. Strong Sulfur Binding with Conducting Magnéli-Phase TinO2n-1 nanomaterials for Improving Lithium-Sulfur Batteries. *Nano Lett.* **2014**, *14* (9), 5288−5294.
(12) Jin, Z.; Xie, K.; Hong, X. Electrochemical Performance of Lithium/Sulfur Batteries Using Perfluorinated Ionomer Electrolyte with Lithium Sulfonyl Dicyanomethide Functional Groups as Functional Separator. *RSC Adv.* **2013**, *3* (23), 8889−8898.
(13) Jin, Z.; Xie, K.; Hong, X.; Hu, Z.; Liu, X. Application of Lithiated Nafion Ionomer Film as Functional Separator for Lithium Sulfur Cells. *J. Power Sources* **2012**, *218*, 163−167.
(14) Ma, L.; Nath, P.; Tu, Z.; Tikekar, M.; Archer, L. A. Highly Conductive, Sulfonated, UV-Cross-Linked Separators for Li-S Batteries. *Chem. Mater.* **2016**, *28* (14), 5147−5154.
(15) Ma, G.; Wen, Z.; Jin, J.; Lu, Y.; Wu, X.; Wu, M.; Chen, C. Hollow Polyaniline Sphere@sulfur Composites for Prolonged Cycling Stability of Lithium-Sulfur Batteries. *J. Mater. Chem. A* **2014**, *2* (27), 10350−10354.
(16) Hyun, J.; Lee, P.; Jung, M.-J.; Ishihara, T. A Simple Preparation of Polyaniline-Coated Sulfur Composites for Use as Cathodes in Li-S Batteries. *Electrochemistry* **2016**, *84* (11), 836−841.
(17) Li, W.; Zhang, Q.; Zheng, G.; Seh, Z. W.; Yao, H.; Cui, Y. Understanding the Role of Different Conductive Polymers in Improving the Nanostructured Sulfur Cathode Performance. *Nano Lett.* **2013**, *13* (11), 5534−5540.
(18) Huang, J. Q.; Zhang, Q.; Peng, H. J.; Liu, X. Y.; Qian, W. Z.; Wei, F. Ionic Shield for Polysulfides towards Highly-Stable Lithium-Sulfur Batteries. *Energy Environ. Sci.* **2014**, *7* (1), 347−353.
(19) Meziane, R.; Bonnet, J. P.; Courty, M.; Djellab, K.; Armand, M. Single-Ion Polymer Electrolytes Based on a Delocalized Polyanion for Lithium Batteries. *Electrochim. Acta* **2011**, *57*, 14−19.
(20) Liao, C.; Sa, N.; Key, B.; Burrell, A. K.; Cheng, L.; Curtiss, L. A.; Vaughey, J. T.; Woo, J. J.; Hu, L.; Pan, B.; et al. The Unexpected Discovery of the $Mg(HMDS)_2$ $MgCl_2$ Complex as a Magnesium Electrolyte for Rechargeable Magnesium Batteries. *J. Mater. Chem. A* **2015**, *3* (11), 6082−6087.
(21) Zhao-Karger, Z.; Zhao, X.; Fuhr, O.; Fichtner, M. Bisamide Based Non-Nucleophilic Electrolytes for Rechargeable Magnesium Batteries. *RSC Adv.* **2013**, *3* (37), 16330−16335.
(22) Wang, J. H. H.; Yang, C. H. C.; Masser, H.; Shiau, H. S.; O'Reilly, M. V.; Winey, K. I.; Runt, J.; Painter, P. C.; Colby, R. H. Ion States and Transport in Styrenesulfonate Methacrylic PEO9 Random Copolymer Ionomers. *Macromolecules* **2015**, *48* (19), 7273−7285.
(23) De Molina, P. M.; Lad, S.; Helgeson, M. E. Heterogeneity and Its Influence on the Properties of Difunctional Poly(Ethylene Glycol) Hydrogels: Structure and Mechanics. *Macromolecules* **2015**, *48* (15), 5402−5411.
(24) Waters, D. J.; Engberg, K.; Parke-Houben, R.; Hartmann, L.; Ta, C. N.; Toney, M. F.; Frank, C. W. Morphology of Photopolymerized End-Linked Poly(Ethylene Glycol) Hydrogels by Small-Angle X-Ray Scattering. *Macromolecules* **2010**, *43* (16), 6861−6870.
(25) Diao, Y.; Helgeson, M. E.; Siam, Z. A.; Doyle, P. S.; Myerson, A. S.; Hatton, T. A.; Trout, B. L. Nucleation under Soft Confinement: Role of Polymer-Solute Interactions. *Cryst. Growth Des.* **2012**, *12* (1), 508−517.
(26) Förster, S.; Timmann, A.; Schellbach, C.; Frömsdorf, A.; Kornowski, A.; Weller, H.; Roth, S. V.; Lindner, P. Order Causes Secondary Bragg Peaks in Soft Materials. *Nat. Mater.* **2007**, *6* (11), 888−893.
(27) Seitz, M. E.; Chan, C. D.; Opper, K. L.; Baughman, T. W.; Wagener, K. B.; Winey, K. I. Nanoscale Morphology in Precisely Sequenced Poly(Ethylene- Co -Acrylic Acid) Zinc Ionomers. *J. Am. Chem. Soc.* **2010**, *132* (23), 8165−8174.
(28) Elmore, C. T.; Seidler, M. E.; Ford, H. O.; Merrill, L. C.; Upadhyay, S. P.; Schneider, W. F.; Schaefer, J. L. Single-Ion Conducting Polymer Electrolytes for Post-Lithium Ion Batteries. *Batteries* **2018**, *4* (2), 28.
(29) Tant, M.; Mauritz, K.; Wilkes, G. *Ionomers: Synthesis, Structure, Properties and Applications*; Blackie Academic and Professional: New York, 2012.
(30) Hall, L. M.; Seitz, M. E.; Winey, K. I.; Opper, K. L.; Wagener, K. B.; Stevens, M. J.; Frischknecht, A. L. Ionic Aggregate Structure in Ionomer Melts: Effect of Molecular Architecture on Aggregates and the Ionomer Peak. *J. Am. Chem. Soc.* **2012**, *134* (1), 574−587.
(31) Gao, T.; Noked, M.; Pearse, A. J.; Gillette, E.; Fan, X.; Zhu, Y.; Luo, C.; Suo, L.; Schroeder, M. A.; Xu, K.; et al. Enhancing the Reversibility of Mg/S Battery Chemistry through Li+Mediation. *J. Am. Chem. Soc.* **2015**, *137* (38), 12388−12393.
(32) Zhou, X.; Tian, J.; Hu, J.; Li, C. High Rate Magnesium−Sulfur Battery with Improved Cyclability Based on Metal−Organic Framework Derivative Carbon Host. *Adv. Mater.* **2018**, *30* (7), 1704166.

DOI: 10.1021/acs.macromol.8b01717
Macromolecules 2018, 51, 8629−8636